Missouri University of Science and Technology
Scholars' Mine

Mechanical and Aerospace Engineering Faculty Research & Creative Works

Mechanical and Aerospace Engineering

01 Jan 2016

Silicon-Wall Interfacial Free Energy via Thermodynamics Integration

Wan Shou

Heng Pan
Missouri University of Science and Technology, hp5c7@mst.edu

Follow this and additional works at: https://scholarsmine.mst.edu/mec_aereng_facwork

Part of the Aerospace Engineering Commons, Mechanical Engineering Commons, and the Numerical Analysis and Scientific Computing Commons

Recommended Citation

W. Shou and H. Pan, "Silicon-Wall Interfacial Free Energy via Thermodynamics Integration," *Journal of Chemical Physics*, vol. 145, no. 18, American Institute of Physics (AIP), Jan 2016.
The definitive version is available at https://doi.org/10.1063/1.4966975

This Article - Journal is brought to you for free and open access by Scholars' Mine. It has been accepted for inclusion in Mechanical and Aerospace Engineering Faculty Research & Creative Works by an authorized administrator of Scholars' Mine. This work is protected by U. S. Copyright Law. Unauthorized use including reproduction for redistribution requires the permission of the copyright holder. For more information, please contact scholarsmine@mst.edu.

Silicon-wall interfacial free energy via thermodynamics integration

Wan Shou and Heng Pan[a)]
Department of Mechanical and Aerospace Engineering, Missouri University of Science and Technology, Rolla, Missouri 65401, USA

(Received 27 July 2016; accepted 21 October 2016; published online 9 November 2016)

We compute the interfacial free energy of a silicon system in contact with flat and structured walls by molecular dynamics simulation. The thermodynamics integration method, previously applied to Lennard-Jones potentials [R. Benjamin and J. Horbach, J. Chem. Phys. **137**, 044707 (2012)], has been extended and implemented in Tersoff potentials with two-body and three-body interactions taken into consideration. The thermodynamic integration scheme includes two steps. In the first step, the bulk Tersoff system is reversibly transformed to a state where it interacts with a structureless flat wall, and in a second step, the flat structureless wall is reversibly transformed into an atomistic SiO_2 wall. Interfacial energies for liquid silicon-wall interfaces and crystal silicon-wall interfaces have been calculated. The calculated interfacial energies have been employed to predict the nucleation mechanisms in a slab of liquid silicon confined by two walls and compared with MD simulation results. *Published by AIP Publishing.* [http://dx.doi.org/10.1063/1.4966975]

I. INTRODUCTION

Manufacture of crystalline silicon wafers typically involves a directional solidification process in order to maximize grain size. The preferred mechanism of silicon crystallization is continuous growth from the solidified region of the crystal without new nucleation at the wall. The interfacial interaction between silicon and the wall material can affect the nucleation behavior[1] and therefore the final grain structure. The nucleation properties of the wall material become especially important when the surface area-to-volume ratio becomes large, such as in zone-melting recrystallization with encapsulating oxide/nitride layers, ribbon growth on substrate, or crystallization on dipped substrate. In addition, the interaction of liquid-wall will also affect the orientation of the crystal.[2] Therefore, it is desirable to understand the Si–SiO_2 interface in order to prevent the undesired nucleation and control the crystal orientation. This article aims at systematic studying of Si–SiO_2 interface in order to predict the nucleation behaviors at these interfaces.

Extensive studies have been devoted to understand the Si–SiO_2 interfacial properties theoretically and experimentally. The interfacial energies concerning silicon only (liquid-crystal, crystal Si, and liquid Si) have been extensively reported. The reported results on Si liquid-crystal interfacial energies are largely consistent. Apte and Zeng[3] employed cleaving wall method for the calculation of anisotropic crystal-melt interfacial free energy of silicon. The cleaving functional form is derived from the repulsive part of the two-body term of the Stillinger-Weber (SW) potential. The calculated liquid-crystal interfacial energies are found to be in 0.34-0.42 J/m^2 range. Si liquid-crystal interfacial energies were also reported by several experimental and simulation works: 0.38 J/m^2 by undercooling experiment,[4] 0.4 J/m^2 by estimation from classical nucleation theory,[5] 0.34 J/m^2 from laser melting experiment,[6] 0.344-0.365 J/m^2 from solidification experiments,[7] 0.43 J/m^2 from contactless cooling experiments,[8] 0.167 J/m^2 using Ginzburg-Landau theory,[9] and 0.413 J/m^2 from MD simulation using SW and Tersoff potentials.[10] It is generally accepted that liquid-crystal interfacial energy is around 0.3-0.4 J/m^2. For liquid silicon interfacial energy, it has been reported to be 0.825 J/m^2,[11] 0.86-0.95 J/m^2,[12] and 0.6 J/m^2 from MD simulation.[13] For crystal Si, it was reported that crystal Si (111) has interfacial energy 0.59-0.83 J/m^2,[14] and higher values 1.23 J/m^2, 1.36 J/m^2, and 1.43 J/m^2 were reported for (111), (100), and (110) surfaces, respectively.[15] Using the available surface energies for Si system, Li was able to conclude that nucleation of free Si slab originates from ~10 to 25 Å below the surface.[13]

The interfacial energies between Si–SiO_2 interfaces (crystal Si–SiO_2 and liquid Si–SiO_2 interfaces) will be more difficult to obtain. For crystal Si–SiO_2, using SW-SiO potential, it is found that the interfacial energy is in the range of 1.15-1.5 J/m^2 between crystal silicon and SiO_2.[16] This is obtained from embedding nanocrystal-Si (nc-Si) in SiO_2 and allowing relaxation to form SiO_{2-x} suboxide layers. Kong used Monte Carlo (MC) simulation to find interfacial energies to be 0.93-1.3 J/m^2 for Si (001)/SiO_2, 1.17-1.75 J/m^2 for Si (110)/SiO_2, and 0.865-1.94 J/m^2 for Si (111)/SiO_2 depending on ionization state of Si.[17] It is found that Si (111) with Si^{+1} ionization state has the lowest interfacial energy. However, Tu used Monte Carlo method to identify a Si (001)-SiO_2 interface with lowest interfacial energy of 0.465 J/m^2,[18] which helps to explain commonly observed (001) orientated crystals on SiO_2 surfaces. For embedded nanocrystal Si in SiO_2, the interfacial energies are 0.8-1.6 J/m^2. For liquid Si–SiO_2 interfaces, the interfacial energy is generally estimated indirectly from contact angle. It is commonly accepted that contact angle is ~87° for a liquid Si droplet and SiO_2 substrate, therefore, the

[a)]Author to whom correspondence should be addressed. Electronic mail: hp5c7@mst.edu

liquid Si–SiO_2 interfacial energy can be estimated indirectly using Young's equation $\gamma_{Si-SiO_2} = \gamma_{SiO_2} - \gamma_{Si}\cos\theta$.

In order to predict the nucleation mechanism during the quenching of a liquid Si in contact with SiO_2 walls, one needs to understand the wetting behaviors of liquid and solid on the walls and have access to the interfacial energies between liquid-wall (γ_{lw}), crystal-wall (γ_{cw}), and liquid-crystal (γ_{lc}). Heterogeneous nucleation (or surface nucleation) requires a crystal partially wets the wall. The macroscopic Young's equation describing a spherical crystal resting on a wall in coexistence with the liquid phase reads $\gamma_{cw} + \gamma_{lc}\cos\theta = \gamma_{lw}$. Partial wetting of the crystal on wall corresponds to contact angle θ in the range from 0 to π or

$$\gamma_{cw} - \gamma_{lw} < \gamma_{lc}. \quad (1)$$

From the above review, there has not been a comprehensive study containing self-consistent values for $\gamma_{cw} - \gamma_{lw}$ and γ_{lc} that are obtained under same simulation or experimental condition, which makes accurate evaluations of Eq. (1) and understanding of nucleation mechanism difficult. Thermodynamic integration (TI) can be used to evaluate the free energy of a given system through a reversible path linking the state of the given system and a state of known free energy.[19] Heni and Löwen[20] developed a TI scheme, where a bulk hard sphere system was reversibly transformed into a system interacting with a more and more impenetrable wall, and finally a hard wall. By combining Monte Carlo (MC) simulations and TI, they were able to obtain the hard sphere liquids (and solids)/ structureless wall interfacial free energies. Later, Fortini and co-workers[21] developed the TI method using an efficient path based on penetrable potentials in exponential form, which gave higher precision in calculation of γ_{cw} and γ_{lw} for hard sphere systems. Cleavage method has been widely used in free energy measurement and calculation both in experiment[22,23] and simulation.[24] Laird and Davidchack developed a TI method by the use of "cleaving potentials," to obtain hard-sphere crystal/liquid interfacial free energies,[25] to obtain Lennard-Jones system crystal/liquid interfacial energies,[26] and to obtain γ_{cw} and γ_{lw} for hard sphere systems at coexistence.[27] Recently, Benjamin and Horbach have applied TI method using pairwise potential with a two-step approach to calculate surface energy between wall-liquid and wall-crystal,[28,29] and crystal-liquid.[30,31] Such interfacial energies have also been combined with experiments to understand and explain heterogeneous nucleation[32–34] and wetting phenomena.[35] In this article, the two-step TI method will be extended for Tersoff potential to calculate interfacial energies for Si–SiO_2 systems. A comprehensive study of these interfacial energies of Si system will be presented based on TI technique aiming at providing consistent explanation of nucleation mechanism during the solidification of liquid Si on SiO_2 walls.

II. MODEL POTENTIAL

The silicon particles are modeled using Tersoff potential,[36]

$$U = \sum_{i=1}\sum_{j>i} V^{II}{}_{i,j} + \frac{1}{2}\sum_{i=1}\sum_{j\neq i} V^{III}{}_{i,j}, \quad (2)$$

with a two-body term $V^{II}{}_{i,j} = f_C(r_{ij})f_R(r_{ij})$ and three-body term $V^{III}{}_{i,j} = f_C(r_{ij})f_A(r_{ij})b_{ij}$. The function f_R represents a repulsive pair potential and f_A represents an attractive potential associated with bonds, f_C is a smooth cutoff function, b_{ij} describes the bond order which is a decreasing function of coordination of atoms i and j, and r_{ij} is distance from atom i to j. The functions f_R, f_A, f_C, and b_{ij} take the following forms:[37]

$$f_R(r_{ij}) = A_{ij}\exp\left(-\lambda_{ij}r_{ij}\right), \quad (3)$$

$$f_A(r_{ij}) = -B_{ij}\exp\left(-\mu_{ij}r_{ij}\right), \quad (4)$$

$$f_C(r_{ij}) = \begin{cases} 1, r_{ij} < R_{ij} \\ \frac{1}{2} - \frac{1}{2}\sin\left(\frac{\pi}{2}\frac{r_{ij}-R_{ij}}{S_{ij}-R_{ij}}\right), R_{ij} < r_{ij} < S_{ij} \\ 0, r_{ij} > S_{ij} \end{cases}, \quad (5)$$

$$b_{ij} = \chi_{ij}\{1 + \beta_i^{n_i}\left[\sum\nolimits_{k\neq i,j} f_C(r_{ik})\,\omega_{ik}\,g(\theta_{ijk})\right]^{n_i}\}^{-\frac{1}{2n_i}}, \quad (6)$$

with

$$g(\theta_{ijk}) = 1 + \frac{c_i^2}{d_i^2} - \frac{c_i^2}{\left[d_i^2 + (h_i - \cos\theta_{ijk})^2\right]}, \quad (7)$$

where θ_{ijk} is the bond angle between bonds ij and ik. All parameters that appear in Eqs. (2)–(7) are tabulated in Table I to describe all the interactions.[37] Hetero-atomic interactions (Si–O) are obtained by set mixing rules,[38] i.e., $A_{ij} = (A_iA_j)^{1/2}$, $B_{ij} = (B_iB_j)^{1/2}$, $R_{ij} = (R_iR_j)^{1/2}$, and $S_{ij} = (S_iS_j)^{1/2}$, while $\lambda_{ij} = \frac{1}{2}(\lambda_i + \lambda_j)$ and.$\mu_{ij} = \frac{1}{2}(\mu_i + \mu_j)$ The parameter χ_{ij} in Eq. (6) is used for tuning the strength of hetero-polar bond and dealing with charge transfer between different atoms. In order to reliably simulate Si nucleation,[13] the original R_{Si} and S_{Si} of Tersoff potential are adopted in current work.[39]

The three-body term V^{III} describes the interaction between two primary atoms i and j which involves the contribution of the third atom k. For the ease of description in this work, we denote the three-body function in the following abbreviated form:

TABLE I. Tersoff potential based parameters for Si–O system.[37,38]

	Si	O
A (eV)	$1.830\,8\times10^3$	$1.882\,55\times10^3$
B (eV)	$4.711\,8\times10^2$	$2.187\,17\times10^2$
λ (Å^{-1})	2.479 9	4.171 08
μ (Å^{-1})	1.732 2	2.356 92
β	$1.100\,0\times10^{-6}$	$1.163\,2\times10^{-7}$
n	$7.873\,4\times10^{-1}$	1.049 68
c	$1.003\,9\times10^5$	$6.469\,21\times10^4$
d	$1.621\,7\times10^1$	4.111 27
h	$-5.982\,5\times10^{-1}$	$-8.459\,22\times10^{-1}$
R (Å)	2.7	1.7
S (Å)	3.0	2.0
ω_{ik}	1	1
χ	$\chi_{Si-Si} = 1$ $\chi_{Si-O} = 1.179\,45$	$\chi_{O-O} = 1$ $\chi_{O-Si} = 1.179\,45$

$$V^{III}{}_{i,j} = V^{III}{}_{i,j}\left(\sum_{k\neq i,j} f(r_{ij}, r_{ik})\right). \quad (8)$$

The TI scheme adopted in this work follows the previous reported method[28] and consists of two steps. First, a bulk Si system (Tersoff) with periodic boundary condition is transformed into an intermediate state where Tersoff system interacts with structureless flat walls (fws). Then, in the second step, the flat walls are reversibly transformed into SiO_2 walls. The structureless flat wall (fw) is a purely repulsive potential interacting along the z direction and is described by the Weeks-Chandler-Anderson (WCA) potential[28]

$$u_{flatwall}(z_i) = \begin{cases} 4\varepsilon\left[\left(\frac{\sigma}{z_i}\right)^{12} - \left(\frac{\sigma}{z_i}\right)^{6} + \frac{1}{4}\right] \times w(z_i), 0 < z_i \leq z_{cw} \\ 0, z_i > z_{cw} \end{cases} \quad (9)$$

with $\varepsilon = 1.0$ eV, $\sigma = 1.7$ Å, the cut-off $z_{cw} = 2^{1/6}\sigma$, and z_i is the distance of particle i to one of the flat walls. The function $w(z_i)$ ensures that $u_{fw}(z_i)$ goes smoothly to zero at $z = z_{cw}$ and is given by

$$w(z_i) = \frac{1}{1 + h^4/(z_i - z_{cw})^4}, \quad (10)$$

where the dimensionless parameter h is set to 0.005.

III. CALCULATION OF INTERFACIAL FREE ENERGIES

A. Hamiltonian, partition functions, and Gibbs free energy

The Hamiltonian of the Tersoff system interacting with a wall, can be written as

$$H(r,p) = \sum_{i=1}^{Np} \frac{1}{2m_i} p_i{}^2 + \sum_{i=1}^{Np}\sum_{j>i}^{Np} V^{II}{}_{i,j} + \frac{1}{2}\sum_{i=1}^{Np}\sum_{j\neq i}^{Np} V^{III}{}_{i,j}\left(\sum_{k\neq i,j}^{Np} f(r_{ij}, r_{ik})\right) + U_{wall}, \quad (11)$$

where p_i is the momentum of atom i, m_i is the mass of atom i, Np is the total number of Si atoms, and U_{wall} is the wall-atom potential. U_{wall} has different forms for flat wall and SiO_2 walls, which are denoted as $U_{flatwall}$ and $U_{SiO_2 wall}$, respectively. The simulation is performed in the NP_NAT ensemble, where the number of particle N, surface area A, and temperature T are kept constant and the length of the simulation box along the z direction is allowed to fluctuate in order to maintain a constant normal pressure P_N. The isothermal-isobaric partition function corresponding the Hamiltonian (11) is[28]

$$Q_{NP_NAT} = \frac{1}{h^{3N}N!}\iiint \exp\left[-\frac{H(r,p) + P_N A L_z}{k_B T}\right] \times A dL_z dr^N dp^N, \quad (12)$$

where r and p denote the position and momentum of the particles, h is the Planck constant, and L_z is the length of the simulation domain in z direction. The Gibbs free energy G of the system is related to the partition function (12) by

$$G = -k_B T \ln Q_{NP_NAT}. \quad (13)$$

Direct calculation of Gibbs free energy using Eqs. (12) and (13) is very difficult. Instead, the following TI approach is taken. To apply TI method, parametrization with λ will be performed.

B. Parametrization with λ and interfacial energy calculated by TI

For interaction with a flat wall, the U_{wall} in Eq. (11) can be written as

$$U_{flatwall} = \sum_{i=1}^{Np} u_{flatwall}(z_i) \quad (14)$$

with the following parametrization of the wall potential with λ:

$$u_{flatwall}(z_i,\lambda) = \lambda^2 4\varepsilon\left[\left(\frac{\sigma}{z_i + (1-\lambda)z_{cw}}\right)^{12} - \left(\frac{\sigma}{z_i + (1-\lambda)z_{cw}}\right)^{6} + \frac{1}{4}\right] w(z_i). \quad (15)$$

At $\lambda = 0$, the Tersoff system can freely cross the boundaries. As λ increases, the wall becomes more and more impenetrable and finally an impenetrable WCA wall is obtained with $\lambda = 1$. The transformation from periodic boundaries to flat walls is accomplished by parametrizing the wall potential as

$$U_{wall}(\lambda) = \sum_{i=1}^{Np} u_{flatwall}(z_i, \lambda).$$

The system Hamiltonian in Eq. (11) parameterized by λ is given by

$$H(r,p,\lambda) = \sum_{i=1}^{Np} \frac{1}{2m_i} p_i{}^2 + \sum_{i=1}^{Np}\sum_{j>i}^{Np} V^{II}{}_{i,j} + \frac{1}{2}\left(\sum_{i=1}^{Np}\sum_{j\neq i}^{Np} V^{III}{}_{i,j}\right)\sum_{k\neq i,j}^{Np} f(r_{ij}, r_{ik}) + U_{wall}(\lambda). \quad (16)$$

The partial derivative of $H(\lambda)$ with respect to λ is given by

$$\frac{\partial H}{\partial \lambda} = \frac{\partial U_{wall}(\lambda)}{\partial \lambda} = \sum_{i}^{Np}\left\{\frac{2}{\lambda} u_{flatwwall}(z_i,\lambda) + \frac{4\varepsilon\lambda^2 z_{cw} w(z_i)}{z_i + (1-\lambda)z_{cw}} \times\left[12\left(\frac{\sigma}{z_i + (1-\lambda)z_{cw}}\right)^{12} - 6\left(\frac{\sigma}{z_i + (1-\lambda)z_{cw}}\right)^{6}\right]\right\}. \quad (17)$$

The derivative of the Gibbs free energy with respect to λ is

$$\frac{\partial G(\lambda)}{\partial \lambda} = -\frac{k_B T}{Q(\lambda)}\left[\frac{\partial Q(\lambda)}{\partial \lambda}\right] = \left\langle \frac{\partial H(\lambda)}{\partial \lambda}\right\rangle_{\lambda}, \quad (18)$$

where the angular brackets denote the ensemble average at a particular value of λ in the NP_NAT ensemble.

The Gibbs free energy difference between the two initial and final states can be written as

$$\Delta G_{iniital->final} = G(\lambda = 1) - G(\lambda = 0) = \int_0^1 \left[\frac{\partial Q(\lambda)}{\partial \lambda}\right] d\lambda = \int_0^1 \left\langle \frac{\partial H(\lambda)}{\partial \lambda}\right\rangle_\lambda d\lambda. \tag{19}$$

The interfacial free energy of a system with walls can be defined as a Gibbs excess free energy per area,

$$\gamma = \frac{G_{system} - G_{bulk}}{A} \tag{20}$$

with G_{system} and G_{bulk} the Gibbs free energies of a system with walls and bulk phase of the system. By this definition, the interfacial energy of system confined by flat walls is

$$\gamma_{si-fw} = \frac{\Delta G_{bulk->fw}}{A}$$

with

$$\Delta G_{si->fw} = \int_0^1 \left\langle \frac{\partial H}{\partial \lambda}\right\rangle_\lambda d\lambda = \int_0^1 \left\langle \frac{\partial U_{wall}(\lambda)}{\partial \lambda}\right\rangle d\lambda. \tag{21}$$

For SiO_2 walls, U_{wall} in Eq. (11) takes the following form:

$$U_{\mathrm{SiO_2}wall} = \sum_{i=1}^{Np}\sum_{j=1}^{Nw} V^{II}{}_{i,j} + \frac{1}{2}\sum_{i=1}^{Np}\sum_{j=1}^{Nw} V^{III}{}_{i,j}\left[\sum_{k\neq i,j}^{Np+Nw} f(r_{ij},r_{ik})\right] + \frac{1}{2}\sum_{i=1}^{Nw}\sum_{j=1}^{Np} V^{III}{}_{i,j}\left(\sum_{k\neq i,j}^{Np+Nw} f(r_{ij},r_{ik})\right) + \left\{\frac{1}{2}\sum_{i=1}^{Np}\sum_{j=1}^{Np} V^{III}{}_{i,j}\left(\sum_{k\neq i,j}^{Np+Nw} f(r_{ij},r_{ik})\right) - \frac{1}{2}\sum_{i=1}^{Np}\sum_{j\neq i}^{Np} V^{III}{}_{i,j}\left(\sum_{k\neq i,j}^{Np} f(r_{ij},r_{ik})\right)\right\} \tag{22}$$

with Nw the total number of atoms in SiO_2 wall (including Si and O atoms), Np the total number of Si atoms in the slab, and $Nw + Np$ the total number of atoms. This equation is used to compute the interactions across the Si-SiO_2 interface. In each loop, the atom index (i, j, or k) loops over all atoms in the group (e.g., Np—all silicon atoms in slab, Nw—all silicon and oxygen atoms in wall, and $Np + Nw$—all atoms). The first term considers all pairwise interactions (Si–Si, Si–O) across the interface. The second and third terms represent three-body interactions with the two primary atoms (i, j) located on different side of the interface. Note the second and the third terms are different due to the sequence in computing the three-body interactions. The fourth term represents the three-body interactions with the two primary atoms (i, j) located in the Si slab. This term is written in a way that only the excessive interactions due to the presence of SiO_2 wall are considered. There is no kinetic energy term for the wall atoms (immobile). Since the SiO_2 wall particles are considered immobile, all the interactions (potential energy) among wall atoms are not included in the above Hamiltonian. In this way, all pairwise and three-body interactions across the interface due to the presence of SiO_2 wall have been considered.

In the second step of TI scheme, the flat wall is reversibly transformed into a SiO_2 wall in contact with liquid silicon. During this change, the SiO_2 walls are positioned at the same location as the flat walls, and there is no interaction between flat and SiO_2 walls. The transformation from flat walls to SiO_2 walls is accomplished by parametrizing the wall potential as

$$\begin{aligned} U_{wall}(\lambda) &= \lambda^2 U_{\mathrm{SiO_2}wall} + (1-\lambda)^2 U_{flatwall} \\ &= \lambda^2\sum_{i=1}^{Np}\sum_{j=1}^{Nw} V^{II}{}_{i,j} + \lambda^2\frac{1}{2}\sum_{i=1}^{Np}\sum_{j=1}^{Nw} V^{III}{}_{i,j}\left(\sum_{k\neq i,j}^{Np+Nw} f(r_{ij},r_{ik})\right) + \lambda^2\frac{1}{2}\sum_{i=1}^{Nw}\sum_{j=1}^{Np} V^{III}{}_{i,j}\left(\sum_{k\neq i,j}^{Np+Nw} f(r_{ij},r_{ik})\right) \\ &\quad + \lambda^2\left\{\frac{1}{2}\sum_{i=1}^{Np}\sum_{j=1}^{Np} V^{III}{}_{i,j}\left(\sum_{k\neq i,j}^{Np+Nw} f(r_{ij},r_{ik})\right) - \frac{1}{2}\sum_{i=1}^{Np}\sum_{j\neq i}^{Np} V^{III}{}_{i,j}\left(\sum_{k\neq i,j}^{Np} f(r_{ij},r_{ik})\right)\right\} + (1-\lambda)^2\sum_{i}^{Np} u_{flatwall}(z_i). \end{aligned} \tag{23}$$

Then the λ-dependent Hamiltonian during the second step of TI is

$$\begin{aligned} H(r,p,\lambda) &= \sum_{i=1}^{Np}\frac{1}{2m_i}p_i{}^2 + \sum_{i=1}^{Np}\sum_{j>i}^{Np} V^{II}{}_{i,j} + \frac{1}{2}\sum_{i=1}^{Np}\sum_{j\neq i}^{Np} V^{III}{}_{i,j}\left(\sum_{k\neq i,j}^{Np} f(r_{ij},r_{ik})\right) \\ &\quad + \lambda^2\sum_{i=1}^{Np}\sum_{j=1}^{Nw} V^{II}{}_{i,j} + \lambda^2\frac{1}{2}\sum_{i=1}^{Np}\sum_{j=1}^{Nw} V^{III}{}_{i,j}\left(\sum_{k\neq i,j}^{Np+Nw} f(r_{ij},r_{ik})\right) + \lambda^2\frac{1}{2}\sum_{i=1}^{Nw}\sum_{j=1}^{Np} V^{III}{}_{i,j}\left(\sum_{k\neq i,j}^{Np+Nw} f(r_{ij},r_{ik})\right) \\ &\quad + \lambda^2\left\{\frac{1}{2}\sum_{i=1}^{Np}\sum_{j=1}^{Np} V^{III}{}_{i,j}\left(\sum_{k\neq i,j}^{Np+Nw} f(r_{ij},r_{ik})\right) - \frac{1}{2}\sum_{i=1}^{Np}\sum_{j\neq i}^{Np} V^{III}{}_{i,j}\left(\sum_{k\neq i,j}^{Np} f(r_{ij},r_{ik})\right)\right\} + (1-\lambda)^2\sum_{i}^{Np} u_{flatwall}(z_i). \end{aligned} \tag{24}$$

The derivative of the Hamiltonian with respect to λ is

$$\frac{\partial H}{\partial \lambda} = \frac{\partial U_{wall}(\lambda)}{\partial \lambda} = 2\lambda \sum_{i=1}^{Np}\sum_{j=1}^{Nw} V^{II}{}_{i,j} + 2\lambda \frac{1}{2}\sum_{i=1}^{Np}\sum_{j=1}^{Nw} V^{III}{}_{i,j}\left(\sum_{k\neq i,j}^{Np+Nw} f(r_{ij},r_{ik})\right) + 2\lambda \frac{1}{2}\sum_{i=1}^{Nw}\sum_{j=1}^{Np} V^{III}{}_{i,j}\left(\sum_{k\neq i,j}^{Np+Nw} f(r_{ij},r_{ik})\right)$$
$$+ 2\lambda\left\{\frac{1}{2}\sum_{i=1}^{Np}\sum_{j=1}^{Np} V^{III}{}_{i,j}\left(\sum_{k\neq i,j}^{Np+Nw} f(r_{ij},r_{ik})\right) - \frac{1}{2}\sum_{i=1}^{Np}\sum_{j\neq i}^{Np} V^{III}{}_{i,j}\left(\sum_{k\neq i,j}^{Np} f(r_{ij},r_{ik})\right)\right\} - 2(1-\lambda)\sum_{i}^{Np} u_{flatwall}(z_i). \tag{25}$$

Finally, using Eqs. (20), (21), and (25), the interfacial free energy of the silicon in contact with a SiO_2 wall is given by

$$\gamma_{\text{Si}-\text{SiO}_2} = \frac{\Delta G_{bulk->fw}}{A} + \frac{\Delta G_{fw->\text{SiO}_2}}{A} \tag{26}$$

with

$$\Delta G_{fw->sio_2} = \int_0^1 \left\langle \frac{\partial H}{\partial \lambda}\right\rangle_\lambda d\lambda = \int_0^1 \left\langle \frac{\partial U_{wall}(\lambda)}{\partial \lambda}\right\rangle d\lambda.$$

On the periodic boundary, the atoms can interact across the boundary with the atoms on the far side of the simulation box. On the periodic boundary, the atoms can exit one end and re-enter the other end. During the first step of TI, the atoms near the wall can interact with the flat wall and the atoms across the periodic boundary.

C. Interfacial free energy calculated by pressure anisotropy

The interfacial free energy can be calculated by employing the Kirkwood and Buff method[40] if the interfacial tension equals the interfacial free energy. This holds for the interfaces between a liquid and flat wall. Hence, we will use interfacial free energy calculated from Kirkwood and Buff method to compare with TI calculated results for liquid-flat wall interfaces. The interfacial surface tension by Kirkwood and Buff method is as follows:

$$\gamma = \frac{1}{2}\int_0^{L_z} \langle P_N(z) - P_T(z)\rangle\, dz, \tag{27}$$

where P_N and P_T are the instant local normal and lateral pressure at z, the bracket indicates ensemble averages, and the factor 1/2 reflects the fact that there are two free surfaces. The instant local normal pressure $P_N(z)$ and lateral pressure $P_T(z)$ are defined as[13]

$$P_N(z) = P_{zz}(z), \tag{28}$$

$$P_T(z) = \frac{1}{2}\left[P_{xx}(z) + P_{yy}(z)\right], \tag{29}$$

and the pressure tensor components $P_{\alpha\alpha}(z)(\alpha = x, y, z)$ are calculated by

$$P_{\alpha\alpha}(z) = \frac{1}{V(z)}\sum_{i\in V(z)} S_{\alpha\alpha,i}, \tag{30}$$

where $V(z)$ is the volume of a sliced slab cut parallel to the surface, and the pressure tensor $P_{\alpha\alpha}(z)$ is calculated by summation of per-atom stress ($S_{\alpha\alpha,i}$) for each atom i within the slice volume then divided by the slice volume.

The per-atom stress $S_{\alpha\alpha,i}$ for atom i is calculated by[41]

$$S_{\alpha\alpha,i} = m_i {v_{\alpha,i}}^2 + \frac{1}{2}\sum_{j\neq i}^{Na}\left(r_{\alpha,i}F_{\alpha,i} + r_{\alpha,j}F_{\alpha,j}\right)$$
$$+ \frac{1}{3}\sum_{k\neq i, j\neq i}^{Nd}\left(r_{\alpha,i}F_{\alpha,i} + r_{\alpha,j}F_{\alpha,j} + r_{\alpha,k}F_{\alpha,k}\right), \tag{31}$$

where the first term is the kinetic energy contribution, the second term is the pairwise contribution where j loops over N_a neighbors of atom i, and the third term is the three-body contribution where j, k loop over all N_d three-body interactions atom i is part of, $v_{\alpha,i}$ is the α components of velocity of atom i, $r_{\alpha,i}$, $r_{\alpha,j}$, and $r_{\alpha,k}$ are the α components of the atom positions, and $F_{\alpha,i}$, $F_{\alpha,j}$, and $F_{\alpha,k}$ are the α components of forces on the atoms. For atoms across the periodic boundary, the r vectors are unwrapped by periodic boundary so that the interacting atoms are close together.[41]

The above pressure tensor only considers interactions among silicon atoms. The additional contribution to the pressure tensor from the structureless flat walls will be taken into account by the Irving and Kirkwood (IK) method.[42] The flat walls are located at z_b and z_t with infinite mass,

$$P_N{}^{flatwall}(z) = \frac{1}{A}\left\langle \sum_{i=1}^{Np} F_{flatwall}(z_i - z_b)\,\Theta(z_i - z)\right\rangle$$
$$- \frac{1}{A}\left\langle \sum_{i=1}^{Np} F_{flatwall}(z_t - z_i)\,\Theta(z - z_i)\right\rangle \tag{32}$$

with $F_{flatwall}(z_i) = -du_{flatwall}(z_i)/dz_i$, and Θ is the Heaviside step function.

IV. BOND ORDER PARAMETER (BOP) COMPUTATION

The method of bond order parameters (BOPs)[43] has been widely used[13,44–47] to identify crystalline atoms from amorphous/liquid atoms and was employed in this study to identify the nucleation during the quenching of a liquid slab. Specifically, local order parameter q_3,[13,44,47] which is sensitive to the crystalline order, was used for Si. The local structure around the atom i is given by

$$\overline{q}_{lm}(i) = \frac{1}{N_b(i)}\sum_{j=1}^{N_b(i)} Y_{lm}\left(\theta\left(\vec{r}_{ij}\right), \varnothing\left(\vec{r}_{ij}\right)\right), \tag{33}$$

where the sum runs over all $N_b(i)$ bonds of atom i, and θ and ∅ denote the azimuthal and polar angles of orientation for bond $\vec{r}_{ij}$.

By constructing a $2l+1$ dimensional vector $\vec{q}_l = [\overline{q}_{l,-l}, \overline{q}_{l,-l+1}, \ldots, \overline{q}_{l,l}]$, we can compute local invariants

$$q_l = \frac{1}{N_b(i)} \sum_{j=1}^{N_b(i)} \frac{\vec{q}_l(i) \cdot \vec{q}_l^{\,*}(j)}{|\vec{q}_l(i)|\,|\vec{q}_l^{\,*}(j)|}. \quad (34)$$

A cutoff distance of 0.293 nm was used to select the nearest neighbor[48] and a cutoff value of $q_{3c} = -0.75$ was adopted to identify crystalline atom from liquid atoms.[44]

V. SIMULATION DETAILS

To integrate the equation of motion, the velocity-Verlet algorithm was used with a time step is 1 fs. The Nose-Hoover thermostat was applied. Constant pressure was applied using the scheme of Shinoda,[49] which combines the hydrostatic equations of Martyna[50] with the strain energy proposed by Parrinello.[51] Periodic boundary conditions were employed in the x y z directions for the first step of the TI method where flat wall was introduced. In the second step of TI, periodic boundary condition was only used along the x and y directions, as illustrated in Fig. 1.

During the first step of TI method, flat walls were applied at the simulation boundary in z direction (LAMMPS[52] allows flat walls imposed simultaneously with periodic boundary condition). The flat walls were physically fixed at the simulation boundary positions. NPT simulation was performed as the strength of the flat wall increases during the first step of TI with the boundary position free to move. At the end of the first step TI method, the periodic boundary condition in z direction was removed. We found the removal of periodic boundary condition has negligible impact on the system energy and surface energy, as pointed out previously.[28] During the second step of TI method, the structured walls (SiO_2) were introduced and fixed at the position of the flat walls. With the increase of the strength of the SiO_2 wall, and positions of the SiO_2 walls must be modified keeping the normal pressure P_N constant. To ensure this, the flat wall (together with SiO_2 structure wall) is changed at every time step to ensure P_N is constant. The individual atoms in the SiO_2 wall were then shifted such that they are at the same relative distance from the center of mass at the beginning of the simulation. To calculate the interfacial free energy via TI, independent simulations were performed at ~40 values of λ between 0 and 1. The number of intervals and the interval spacing were selected to ensure a smooth profile for the thermodynamic integrand and ensure further increase of the number of intervals does not change the integration results significantly. Fewer points were used where the curve changes gradually and more dense points were placed where curve changes rapidly. At each λ, $1 \times 10^5 - 1 \times 10^6$ time steps were allowed to reach equilibrium before 1×10^5 time steps for data averaging were performed. The data were stored every 100 time steps and a total of 1000 configurations were collected to calculate the averaged values. Three independent runs were performed and standard deviation was obtained from the independent runs to evaluate the variations and errors of the above described TI scheme. The trapezoidal rule was used for integration in each independent run,

$$\Delta G = \sum_{i=1}^{N_\lambda - 1} \frac{1}{2} \left[\left\langle \frac{\partial H}{\partial \lambda} \right\rangle_i + \left\langle \frac{\partial H}{\partial \lambda} \right\rangle_{i+1} \right] (\lambda_{i+1} - \lambda_i). \quad (35)$$

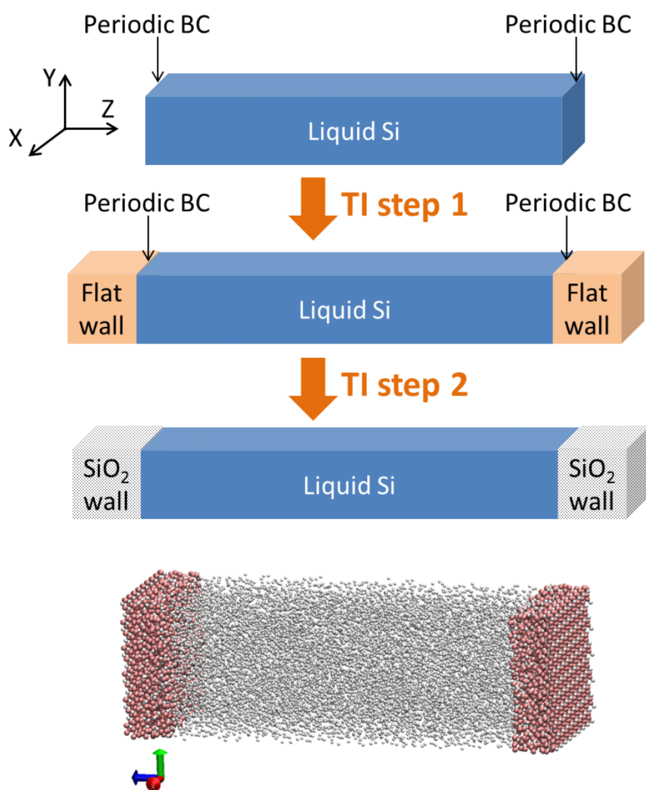

FIG. 1. MD simulation configuration and the two-step thermodynamic integration scheme.

In this current study, no chemical reactions, such as oxidation or reduction, with surrounding gas will be allowed during TI process. The interaction between liquid Si and solid silicon to form gaseous compound SiO is neglected.[35,53] The SiO_2 substrate will be prepared before simulation and is considered fixed and immobile during the TI process. Sufficient interactions are allowed between Si–Si and Si–O atoms across the interface as described by Tersoff potential.[37] Since the interface energies will be strongly depending on bonds and interaction of un-passivated Si and O atom from SiO_2 substrate, we follow the following procedures to prepare SiO_2 substrate surface and Si solid in this study.

For SiO_2 surface, we did not attempt to prepare accurate reconstructions of crystalline or amorphous SiO_2 surface. We focus on evaluating the TI methodology to calculate interfacial energies and verify the interfacial energies by nucleation simulations. Thus, this methodology should be applicable for any arbitrary SiO_2 substrate. Therefore, we use an "arbitrary" approach to prepare SiO_2 substrates. An α-quartz crystal slab cut along (001) plane with silicon terminated surface and an area of 2500 Å^2 and thickness of 15 Å was selected. Only the surface atoms (10 Å) were allowed to relax by NPT at 1800 K for 2×10^6 steps, and the sub-surface atoms (5 Å) were fixed during the NPT relaxation. The prepared SiO_2 surfaces are shown in Fig. 2.

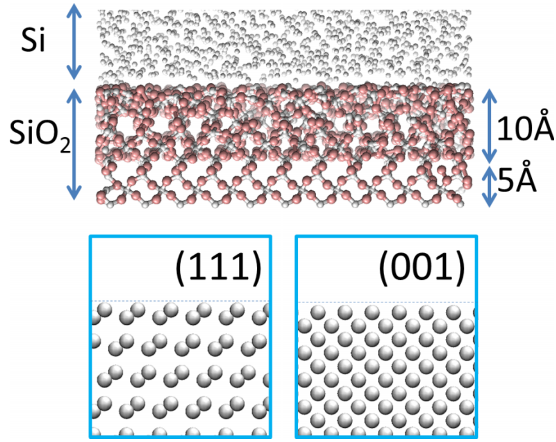

FIG. 2. The interfacial configuration between Si and SiO_2 (up) and selected Si crystal surfaces (down).

For Si solid surface, we limit our focus to (111) and (001) surfaces since it has been determined the orientation on these two directions provides lowest interfacial energies (typically (110) is not the lowest). We have prepared the (001) and (111) silicon crystal surfaces with different ionization states. For flat surfaces, the ionization state of the Si atoms depends on where the Si atoms are cleaved. For Si (001), the only possible state is Si^{+2} as shown in Fig. 2. For Si (111), there are two possibilities, Si^{+1} and Si^{+3}. It is reported that the energy of Si (111)[Si^{+1}]/a-SiO_2 interface has the lowest interfacial energy.[17] Thus we have chosen the Si^{+1} for (111) due to lowest energies reported. The selected Si crystals are shown in Fig. 2.

In performing simulations of crystal in contact with walls on both sides, the number of particles must be chosen such that it is compatible with the long-range order of the crystal. The simulation dimensions are chosen properly for (111) and (100) in order to maintain the long-range order. The simulation dimensions and total number of atoms in Table II are used. The simulations of liquid Si use the initial configuration of solid (111).

Figure 3(a) shows the thermodynamic integrand as a function of λ during the transformation of a bulk liquid (solid) to a confined liquid (solid) interacting with flat walls. The integrand is smooth, allowing for an accurate determination of the interfacial free energy. Figures 3(b) and 3(c) show

TABLE II. The simulation dimensions for TI calculation of solid Si with confining walls.

	X dimension (Å)	Y dimension (Å)	Z dimension (Å)	Atom number
(111)	46.083	46.561	112.881	12 495
(100)	48.879	48.879	135.775	16 200

the integrands as a function of λ for the second step of the thermodynamic integration when the flat wall is transformed into a structured wall. The integrand is always negative, which implies the interfacial free energy of a Si liquid (solid) in contact with a rigid structured SiO_2 wall is smaller than for the case where the liquid (solid) Si is in contact with a structureless flat wall.

VI. RESULTS

A. Liquid-flat wall interfacial energy

Using TI, we first determine the liquid-flat wall interfacial free energies at several temperatures and pressures, as plotted in Fig. 4. The liquid-wall interfacial free energies decrease with increase in temperature. The melting point T_m of Tersoff model is 2567 K,[10] which is higher than experimental value 1683 K. With P_N = 1000 bars, the liquid-flat wall interfacial energy calculated at 2600 K is ~0.68 J/m^2. This value is in reasonable agreement with 0.65 J/m^2 as calculated by Kirkwood-Buff method. The values from the present study are slightly higher than the liquid Si-vacuum interfacial energy (0.6 J/m^2) reported by Li for Tersoff potential at T = 0.95 T$_m$.[13] It appears the introduction of confining walls increases the interfacial energy. By increasing the confining pressure to 10 000 bars, the liquid-wall interfacial free energies increase to ~0.89 J/m^2.

The difference between TI and Kirkwood-Buff calculated surface energy, as seen in Fig. 4(b), can be due to pressure fluctuation. Figures 4(c) and 4(d) show the normal pressure and tangential pressure for two confining pressures. Large fluctuation in both normal and tangential pressure profiles in the bulk region can be seen. Since pressure calculation uses the difference between two pressure profiles, any lack of precision

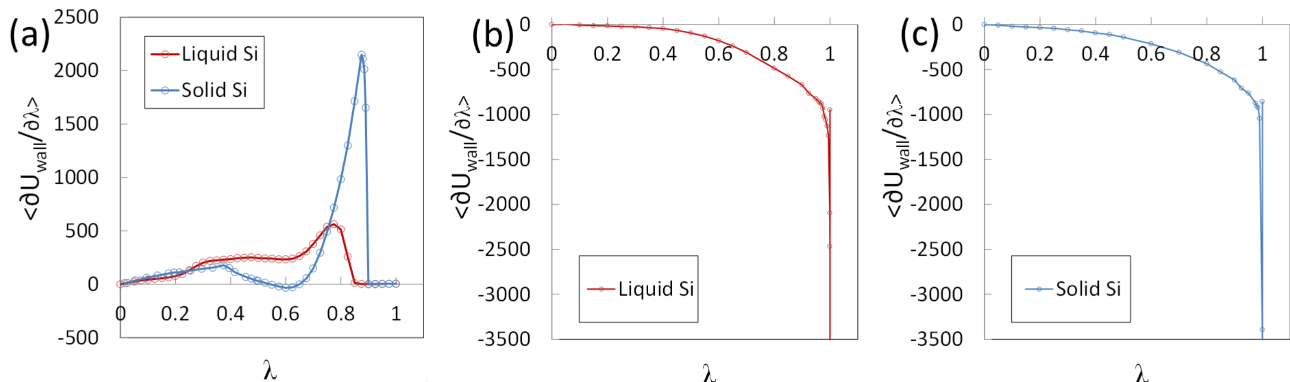

FIG. 3. The thermodynamic integrand during TI steps. (a) Step 1-bulk to flat walls transition. Step 2-flat wall to SiO_2 wall transition for liquid Si (b) and solid Si (c).

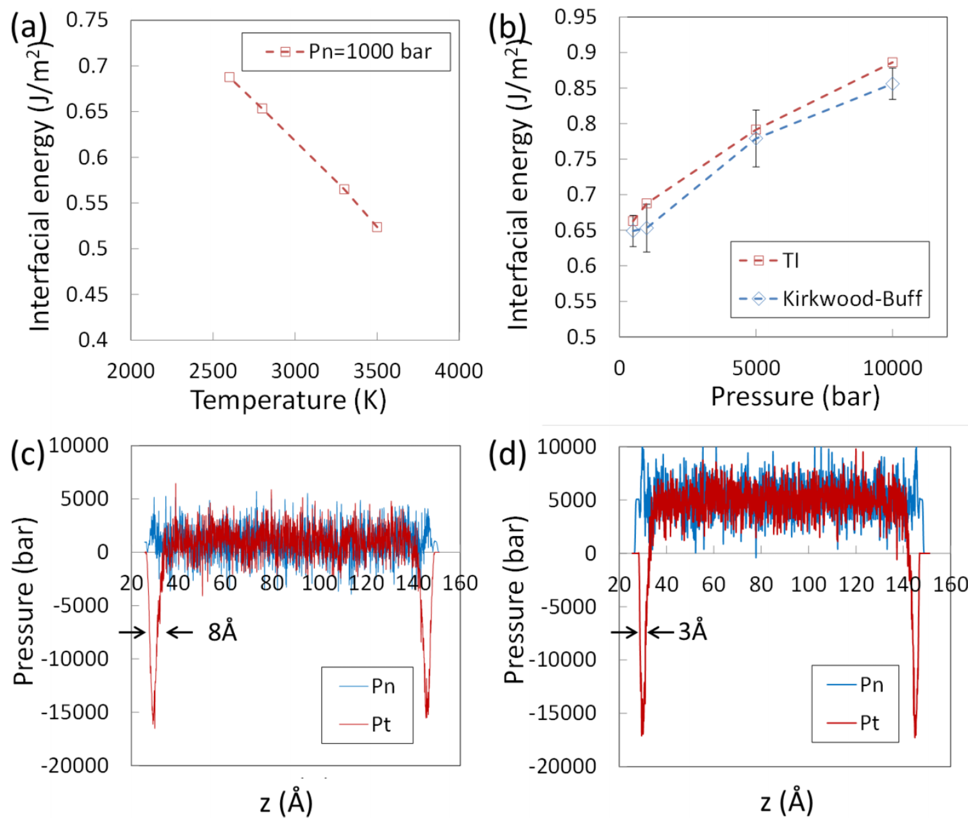

FIG. 4. The interfacial energies between liquid Si and flat walls for different confining pressure (a) and temperature (b). Calculated normal and tangential pressure components under 1000 bars (c) and 5000 bars (d) confining pressures.

in the numerical measurements magnifies the relative error. The error in Kirkwood-Buff calculated surface energies is estimated from the fluctuation and included in Figs. 4(c) and 4(d). It should be pointed out that there is a negative pressure region near the surface. The normal confining pressure alters the width of negative pressure regions. The width decreases from 8 Å to 3 Å as confining pressure increases.

B. Solid-flat wall interfacial energy

The solid-flat wall interfacial energies are calculated and shown in Fig. 5(a). We will firstly focus on close packed (111) orientation of the crystal in contact with a flat wall. In Fig. 5(a), we plot interfacial energy between solid Si (111) with a flat wall, as a function of temperature up to the liquid-solid coexistence temperature at P_N = 1000 bars. For comparison, interfacial energies between liquid Si with a flat wall are also plotted in the same plot. All the interfacial energies decrease with increasing in temperature. The interfacial energies near melting temperature for liquid and solid Si in contact with flat wall are labeled as γ_{lw} and γ_{cw}, respectively.

The values of γ_{lw} and γ_{cw} (the interfacial energies near melting temperature) were computed for various confining pressures and plotted in Fig. 5(b). It is found $\gamma_{cw} - \gamma_{lw}$ decreases monotonically with increasing confining pressure. With the confining pressure P_N = 500 bars, $\gamma_{cw} - \gamma_{lw}$ is ~0.272 J/m^2. The asymptotic value of $\gamma_{cw} - \gamma_{lw}$, as confining pressure decrease, can be estimated to be ~0.3 to 0.4 J/cm^2. It is generally accepted that for Tersoff potential, γ_{lc} is 0.34–0.41 J/m^2.[10] Thus, in a liquid Si slab weakly confined by flat walls, $\gamma_{cw} - \gamma_{lw} \sim \gamma_{lc}$, which suggests nucleation originating from the interface (or heterogeneous nucleation) is not energetically favored. If free surface could be

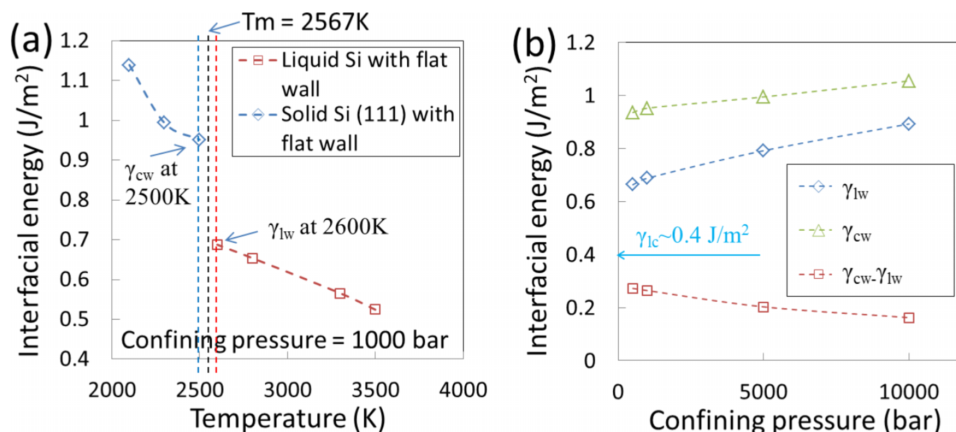

FIG. 5. (a) The interfacial energies between solid Si (111) and flat walls for different temperatures. The interfacial energies between liquid Si and flat walls are also included for comparison. (b) The interfacial energies of liquid-wall and solid-wall near melting temperature under different confining pressures.

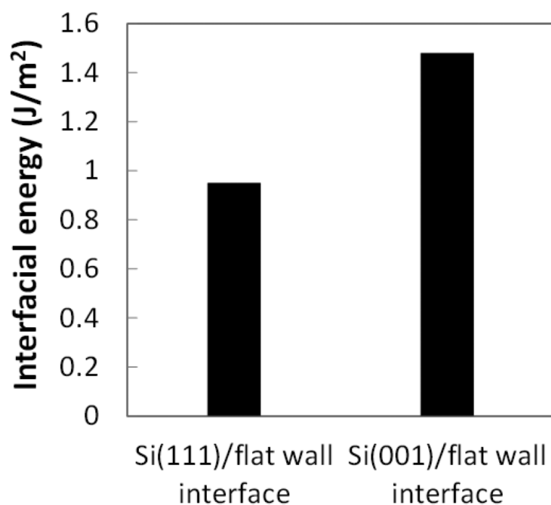

FIG. 6. The interfacial energies between different orientated Si crystals with flat wall.

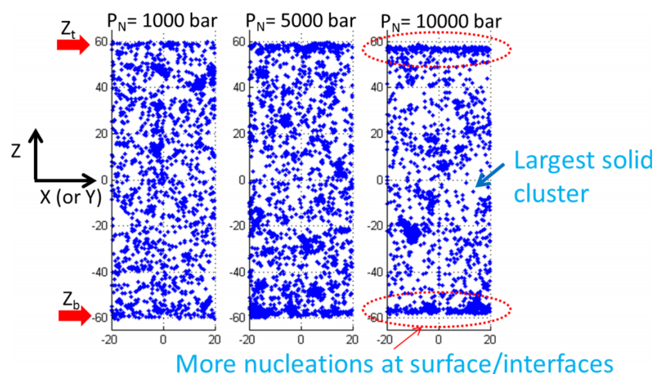

FIG. 7. The distribution of nucleus in the slab under different confining pressures.

approximated as weakly confined slab, current result is in agreement with free surface nucleation study by Li suggesting nucleation is not originated from free surfaces.[13] In Fig. 5(b), it is noticed that by increasing the confining pressure, $\gamma_{cw} - \gamma_{lw}$ decreases from 0.272 to 0.168 J/m^2, which is much less than reported γ_{lc}. Thus, one can expect that the heterogeneous nucleation will occur in a slab at high confining pressure. The verification of this conclusion will be discussed in Sec. VI C.

The interfacial energy between differently orientated solid Si on flat walls was computed and plotted in Fig. 6. It shows that the interfaces between Si (111) and flat surface are lower than that between Si (100) and flat surface.

To test any finite-size effects, we performed additional simulations with different system sizes. It has been suggested that systems of 4000 atoms are large enough to avoid finite size effects in the calculation of interfacial free energies.[28] We calculate γ_{lw} in larger (26 250 atoms—$69.12 \times 66.515 \times 112.881$ Å^3) and smaller (6048 atoms—$30.722 \times 33.257 \times 112.881$ Å^3) systems. The computed value γ_{lw} increases by ~2% from the smallest system to the largest system. The increase of computed γ_{lw} from 12 495 atoms to 26 250 atoms is only ~0.5%. Therefore, it is believed with system size at 12 495 atoms, finite size is marginal in this work. A more systematic finite size analysis will be carried out in future work to understand the variation with respect to system size.

C. Crystallization on flat walls

In order to verify the predicted nucleation mechanism of liquid Si confined by flat walls under different confining pressures, the crystallization was monitored using the BOP method during a quenching process. The temperature was linearly ramped down from 2600 K to 1000 K within 5 ns. There are a total of 5000 samplings performed during the quenching. In each sampling, the size and location of the largest solid cluster in the liquid slab, as computed by BOP, was recorded and plotted in Fig. 7. Each scatter point in Fig. 7 represents the location of the largest cluster during one sampling. By increasing confining pressure, more nucleation occurs at the wall surface. The preferred nucleation on the interface/surface is contributed to the lower surface energies difference $\gamma_{cw} - \gamma_{lw}$ as concluded from TI computation previously.

D. Liquid Si–SiO_2 wall and solid Si–SiO_2 wall interfacial energy

The liquid-flat wall system can now be used as the reference system to calculate the interfacial free energy of the liquid in contact with a rigid SiO_2 wall. The external pressure is set to 1000 bars and the temperature to 2600 K. The thermodynamic integrand plots are shown for liquid and solid Si on the SiO_2 substrates in Figs. 8(a) and 8(b). It is found that the integrand curve shows a large kink with λ close to 1. We adopted very fine steps near λ close to 1 and performed long equilibrium runs (up to 4×10^6 steps). It is found that

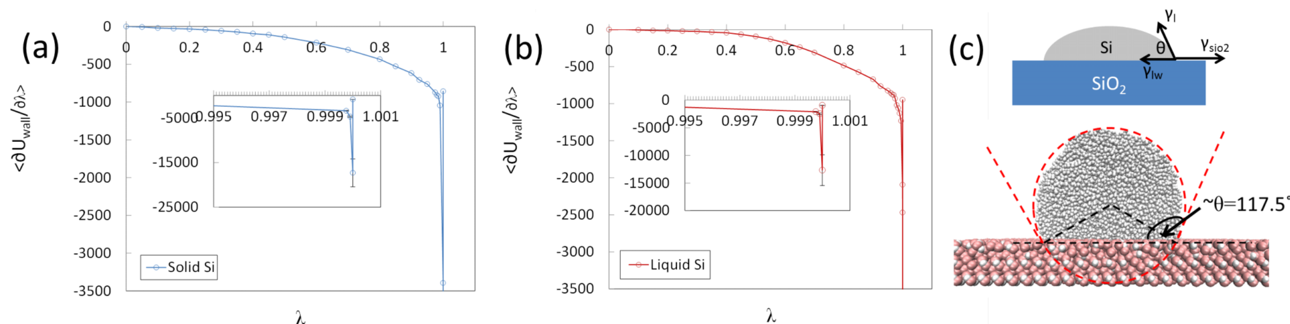

FIG. 8. The thermodynamic integrand during TI step 2-flat wall to SiO_2 wall transition for liquid-Si (a) and solid-Si (b) interfaces. (c) Direct simulated liquid Si droplet on SiO_2 substrate.

significant kink appears only with $\lambda > 0.9999(\lambda = 0.999\,999)$, as shown in the insets of Figs. 8(a) and 8(b). Since the kink only occurs in a very small interval of λ, it has minor impact on the final results (i.e., removing the point at $\lambda = 0.999\,999$ only induces <0.1% variation). Therefore, we conclude the presence of kink very close to $\lambda = 1$ has negligible effects if sufficiently fine steps are used near $\lambda = 1$. The kinks are due to extremely large value of $\sum_i^{Np} u_{flatwall}(z,1)$ (the last term in in Eq. (25)) when $\lambda \sim 1$. It is believed that with λ approaching 1, the flat wall becomes very weak. Meanwhile, the atoms interact strongly with SiO_2 wall. Due to the atomic level un-evenness of the SiO_2 walls, the atoms could be very close to the perfectly flat wall, which gives rise to the large $\sum_i^{Np} u_{flatwall}(z,1)$ values. Since the term $\sum_i^{Np} u_{flatwall}(z,1)$ increases nonlinearly with $(1-\lambda)$, multiplying this term with $(1-\lambda)$ is not able to negate this effect. Other parameterizations could be more effective in removing the kinks and will be studied in the future work.

Using the integrand for liquid, γ_{lw} is found to be -0.202 J/m^2. The negative value is due to the strong interaction between liquid Si and O atoms in the substrate. The enthalpy of formation between Si and O is −476 kJ per atom of O.[53] To understand physical implication of the obtained γ_{lw} value, we will consider the contact angle of a liquid Si droplet on SiO_2 substrate (Fig. 8(c)). The surface energy of liquid Si (γ_l) can be estimated to be 0.68 J/m^2 from Fig. 4(a) or previous results.[13] Since the solid SiO_2 walls are considered to be immobile in this study, it is assumed that $\gamma_{sio2} = 0$. According to Young's equation $\gamma_{SiO_2} = \gamma_l \cos\theta + \gamma_{lw}$, it can be found that the contact angle is ∼72.8°, which is in agreement with commonly accepted contact angle of a liquid Si droplet on SiO_2 substrates. To verify the contact angles, we perform the direct simulation of liquid Si droplet on the substrate and equilibrium contact angle was obtained after 10 ns equilibrium (Fig. 8(c)). Similar to the reported procedure based on the contour of the droplet,[54] we fit the outline of a liquid Si droplet using a circle, then the contact angle was defined as the angle between a tangential line of the outline through a three-phase contact point and another line on the flat surface going through the three-phase contact point. The final contact angle is averaged from 8 measurements (in the range 104°-123°) to be ∼117.5°, higher than Young's equation prediction using TI calculated values ∼72.8°. The deviation from Young's equation could be expected due to the contribution of line tension effects in nanodroplets,[55–57] and the dependence of γ_{lw} on pressure (Fig. 5(b)). The work of adhesion $W = \gamma_l(1 + \cos\theta)$ can be estimated to be ∼0.881 J/m^2 which is found to be close to experimentally measured values 0.86 J/m^2 for silicon on silica as measured from sessile-drop method.[43] From the contact angle and work of adhesion calculation, we conclude the arbitrarily prepared SiO_2 substrate is physical and can be used for crystallization study.

Using the TI integrand for solid silicon in contact with the SiO_2 walls (Fig. 8(a)), γ_{cw} is found to be 0.006 91 J/m^2. Using the aforementioned $\gamma_{lw} = -0.202$ J/m^2, it is found $\gamma_{cw} - \gamma_{lw}$ for Si on SiO_2 substrate is 0.209 J/m^2, slightly lower than $\gamma_{lc} \sim 0.34$ to 0.4 J/m^2 as reported previously. Our TI calculation indicates weak heterogeneous nucleation will occur during the cooling of liquid Si in contact with the SiO_2 substrate, as will be discussed next.

E. Crystallization on SiO_2 walls

The spatial distributions of the largest clusters during cooling in a slab confined by SiO_2 walls and an un-confined slab (free surface) are compared in Fig. 9. The most prominent difference is the appearance of more large clusters (>20 atoms) in the wall confined slab. In particular, there are more large clusters found near the interface/surface region, as indicated by the red dashed circles in Fig. 9(b). It is also found that for wall-confined slab, clusters with atom # >10 are absent in the region immediately (<10 Å) below the interface, as indicated by the blue dashed circles. The absence of crystalline Si cluster immediately adjacent to SiO_2 substrate is due to the crystalline disorder introduced by SiO_2 surfaces. To verify this, we perform BOP analysis to identify crystalline Si (colored cyan) of a perfect Si (111) film in contact with SiO_2 surface. It is found a transition layer with thickness ∼5 to 10 Å cannot be recognized as crystalline Si (colored white). Thus, it is suggested that compared with free surface slab, in SiO_2 confined slab, there are more Si clusters formed near the surface region. The interfacial energies calculated by current TI method serve the purpose to explain the enhanced nucleation near Si–SiO_2 interfaces.

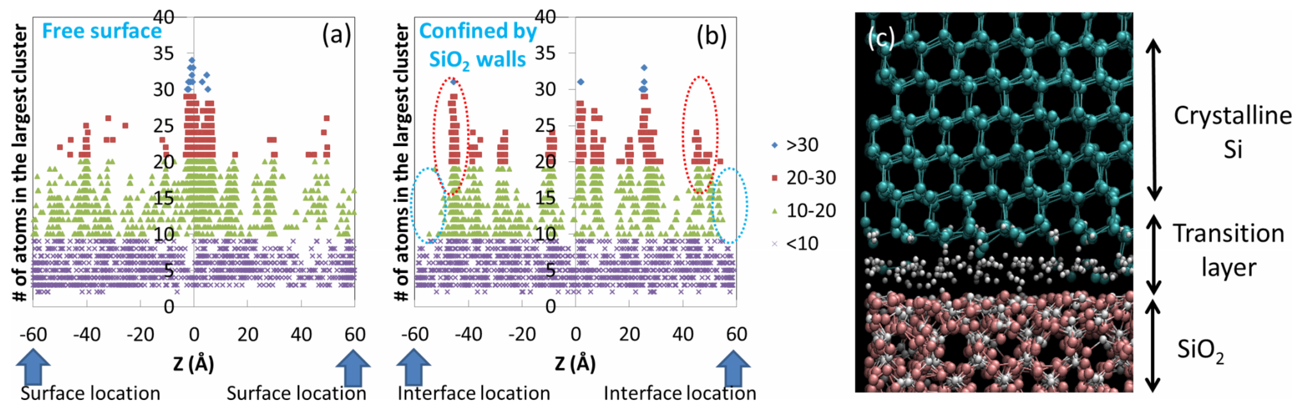

FIG. 9. The location and size of the largest cluster during the cooling simulation of un-confined slab (a) and SiO_2 wall confined slab (b). (c) The crystalline structure at the solid Si–SiO_2 interface. The "crystalline" Si is colored cyan and "non-crystalline" Si is colored white.

VII. CONCLUSION

A thermodynamics integration method to compute the interfacial free energy of a silicon system in contact with flat structureless walls and structured SiO_2 walls by molecular dynamics simulation is described. The method has been employed to calculate interfacial energies for liquid and solid silicon in contact with flat and structured walls. The method provides simple and reliable estimates of γ_{cw} and γ_{lw} that can be used with Young's equation to evaluate wettability and nucleation mechanisms. Most importantly, the method provides a general approach to calculate anisotropic crystal-wall interfacial energies for real material systems, which are hardly accessible in experiments and highly important to interpret experimental observations. The results have been used to predict and explain the observed nucleation mechanism during the quenching of a liquid Si slab confined by walls, and agreement with direct MD simulation results has been found.

ACKNOWLEDGMENTS

This work was supported by the National Science Foundation under Grant No. 1363313. This work was also partially supported by ORAU Ralph E. Powe Junior Faculty Enhancement Award. Their financial support is greatly appreciated.

[1]A. T. Appapillai, C. Sachs, and E. M. Sachs, J. Appl. Phys. **109**, 084916 (2011).
[2]K. Fujiwara, K. Maeda, H. Koizumi, J. Nozawa, and S. Uda, J. Appl. Phys. **112**, 113521 (2012).
[3]P. Apte and X. C. Zeng, Appl. Phys. Lett. **92**, 221903 (2008).
[4]Y. Shao and F. Spaepen, J. Appl. Phys. **79**, 2981 (1996).
[5]R. P. Liu, T. Volkmann, and D. M. Herlach, Acta Mater. **49**, 439 (2001).
[6]S. R. Stiffler, M. O. Thompson, and P. S. Peercy, Phys. Rev. Lett. **60**, 2519 (1988).
[7]P. V. Evans and S. R. Stiffler, Acta Metall. Mater. **39**, 2727 (1991).
[8]D. Li and D. M. Herlach, Europhys. Lett. **34**, 423 (1996).
[9]X. C. Zeng and D. Stroud, J. Phys.: Condens. Matter **1**, 1779 (1989).
[10]Y. W. Tang, J. Wang, and X. C. Zeng, J. Chem. Phys. **124**, 236103 (2006).
[11]X. Huang, S. Togawa, S. I. Chung, K. Terashima, and S. Kimura, J. Cryst. Growth **156**, 52 (1995).
[12]Z. Q. Wang and D. Stroud, Phys. Rev. B **38**, 1384 (1988).
[13]T. Li, D. Donadio, L. M. Ghiringhelli, and G. Galli, Nat. Mater. **8**, 726 (2009).
[14]J. J. Métois and P. Müller, Surf. Sci. **548**, 13 (2004).
[15]D. J. Eaglesham, A. E. White, L. C. Feldman, N. Moriya, and D. D. Jacobson, Phys. Rev. Lett. **70**, 1643 (1993).
[16]F. Djurabekova and K. Nordlund, Phys. Rev. B **77**, 115325 (2008).
[17]L. Kong and L. J. Lewis, Phys. Rev. B **77**, 085204 (2008).
[18]Y. Tu and J. Tersoff, Phys. Rev. Lett. **84**, 4393 (2000).
[19]D. Frenkel and B. Smit, *Understanding Molecular Simulation* (Academic, San Diego, 2002).
[20]M. Heni and H. Löwen, Phys. Rev. E **60**, 7057 (1999).
[21]A. Fortini and M. Dijkstra, J. Phys.: Condens. Matter **18**, L371 (2006).
[22]J. J. Gilman, J. Appl. Phys. **31**, 2208 (1960).
[23]J. P. Berry, J. Appl. Phys. **34**, 62 (1963).
[24]J. Q. Broughton and G. H. Gilmer, J. Chem. Phys. **84**, 5759 (1986).
[25]R. L. Davidchack and B. B. Laird, Phys. Rev. Lett. **85**, 4751 (2000).
[26]R. L. Davidchack and B. B. Laird, J. Chem. Phys. **118**, 7651 (2003).
[27]B. B. Laird and R. L. Davidchack, J. Phys. Chem. C **111**, 15952 (2007).
[28]R. Benjamin and J. Horbach, J. Chem. Phys. **137**, 044707 (2012).
[29]R. Benjamin and J. Horbach, J. Chem. Phys. **139**, 084705 (2013).
[30]R. Benjamin and J. Horbach, J. Chem. Phys. **141**, 044715 (2014).
[31]R. Benjamin and J. Horbach, Phys. Rev. E **91**, 032410 (2015).
[32]K. Sandomirski, S. Walta, J. Dubbert, A. Allahyarov, A. B. Schofield, H. Löwen, W. Richtering, and S. U. Egelhaaf, Eur. Phys. J.: Spec. Top. **223**, 439 (2014).
[33]A. Reinhardt and J. P. K. Doye, J. Chem. Phys. **141**, 084501 (2014).
[34]J. Bokeloh, G. Wilde, R. E. Rozas, R. Benjamin, and J. Horbach, Eur. Phys. J.: Spec. Top. **223**, 511 (2014).
[35]L. D. Alphei, R. Grotjahn, C. Dobbe, M. Douvidzon, R. Janhsen, T. Gebensleben, T. Alznauer, V. Becker, and J. A. Becker, J. Cryst. Growth **419**, 165 (2015).
[36]J. Tersoff, Phys. Rev. B **39**, 5566 (1989).
[37]S. Munetoh, T. Motooka, K. Moriguchi, and A. Shintani, Comput. Mater. Sci. **39**, 334 (2007).
[38]C. Y. Chuang, Q. M. Li, D. Leonhardt, S. M. Han, and T. Sinno, Surf. Sci. **609**, 221 (2013).
[39]B. M. Lee, T. Motooka, and S. Munetoh, J. Phys.: Condens. Matter **20**, 055205 (2008).
[40]J. G. Kirkwood and F. P. Buff, J. Chem. Phys. **17**, 338 (1949).
[41]A. P. Thompson, S. J. Plimpton, and W. Mattson, J. Chem. Phys. **131**, 154107 (2009).
[42]J. H. Irving and J. G. Kirkwood, J. Chem. Phys. **18**, 817 (1950).
[43]P. J. Steinhardt, D. R. Nelson, and M. Ronchetti, Phys. Rev. B **28**, 784 (1983).
[44]T. Li, D. Donadio, and G. Galli, J. Chem. Phys. **131**, 224519 (2009).
[45]H. Pan and C. P. Grigoropoulos, J. Appl. Phys. **115**, 104307 (2014).
[46]H. Pan and W. Shou, J. Phys. D: Appl. Phys. **48**, 225302 (2015).
[47]L. M. Ghiringhelli, C. Valeriani, E. J. Meijer, and D. Frenkel, Phys. Rev. Lett. **99**, 055702 (2007).
[48]S. Sastry and C. A. Angell, Nat. Mater. **2**, 739 (2003).
[49]W. Shinoda, M. Shiga, and M. Mikami, Phys. Rev. B **69**, 134103 (2004).
[50]G. J. Martyna, D. J. Tobias, and M. L. Klein, J. Chem. Phys. **101**, 4177 (1994).
[51]M. Parrinello and A. Rahman, J. Appl. Phys. **52**, 7182 (1981).
[52]S. Plimpton, J. Comput. Phys. **117**, 1 (1995).
[53]R. Sangiorgi, M. L. Muolo, D. Chatain, and N. Eustathopoulos, J. Am. Ceram. Soc. **71**, 742 (1988).
[54]T. Werder, J. H. Walther, R. L. Jaffe, T. Halicioglu, F. Noca, and P. Koumoutsakos, Nano Lett. **1**, 697 (2001); T. Koishi, K. Yasuoka, S. Fujikawa, and X. C. Zeng, ACS Nano **5**, 6834 (2011); Y. Li, F. Wang, H. Liu, and H. Wu, Microfluid. Nanofluid. **18**, 111 (2015).
[55]P. G. de Gennes, Rev. Mod. Phys. **57**, 827 (1985).
[56]T. Getta and S. Dietrich, Phys. Rev. E **57**, 655 (1998); L. Schimmele and S. Dietrich, Eur. Phys. J. E **30**, 427 (2009).
[57]D. Winter, P. Virnau, and K. Binder, Phys. Rev. Lett. **103**, 225703 (2009); J. K. Berg, C. M. Weber, and H. Riegler, *ibid.* **105**, 076103 (2010); J. H. Weijs, A. Marchand, B. Andreotti, D. Lohse, and J. Snoeijer, Phys. Fluids **23**, 022001 (2011).